Korean J. of Chem. Eng., **7**(4) (1990) *296-305*

EFFECT OF PORE STRUCTURE ON SO_2 ADSORPTION EFFICIENCY

Chan-Young PARK*, Yong-Choon LEE, Soo Hyun CHUNG and Eun-San SOHN**

Department of Fine Chemical Engineering, Chonnam National University,
Kwangju 500-757, Korea
**Korea Institute of Energy & Resources

(Received 6 July 1990•accepted 23 October 1990)

Abstract—The influence of the impregnation concentration of copper nitrate in a porous alumina pellet on the SO_2 adsorption efficiency has been investigated. The mechanism of adsorption and pore clogging has been analysed on the basis of the partitioned pore structure model and the results has been compared with the experimental breakthrough curves.

The complete conversion of the pellet was attained in the low concentration of impregnation. The breakthrough time could be increased by increasing the concentration in the range from 2.0 to 6.0 mol/l copper nitrate solution when the SO_2 concentration was about 3000 ppm. The conversion rate, however, dropped rapidly as the pore clogging occurred at the higher concentration than the optimum level.

INTRODUCTION

Reducing sulfur dioxide emission from electric power plants has attracted a great deal of attention, and various flue gas desulfurization (FGD) processes for such plants have been developed. Among the processes, dry flue gas desulfurization using regenerative solid materials would be advantageous since they might produce useful by-products and avoid reheating the vent gas for drifting into atmosphere. In one of these process [1] the flue gas is brought into contact with spheres of cupric oxide-impregnated alumina whereupon SO_2 at low concentration less than one percent reacts to produce copper sulfate. A considerable advantage of this process is the readiness with which copper oxide may be regenerated at the same temeperature with reducing gas such as hydrogen or light alkane [2].

Many factors can play a role in the economics of FGD. The contents of metal oxides in supports govern the completeness of reaction that is imperative with the needs for decreasing the manufacturing cost of adsorbent and for the maximum use of the reactant. The adsorbent must have the commensurated pore structure. Even if the structure is good initially for the diffusion of SO_2, the reaction between the gas and the solid may alter the pore shape resulting in shrinking the radius of pore, and may finally close the pore entrance. Chung et al. [3] concluded that the cupric oxide had to be impregnated in a proper solution concentration to achieve the maximum conversion. They estimated the shrinking rate of root mean averaged pore radius along with reaction progress, and proposed a simplified model by which changes of the thickness of product layer with time could be estimated. Simons and Rawlins [4] developed a simple theory describing the mass transport and the heterogeneous chemistry which occurs when either SO_2 or H_2S reacts with the calcined limestone. The conspicuous distinction in the reaction scheme between the limestone-like sorbents and the metal oxide impregnated sorbents is that restrictions exist for the impregnated ones while no restrictions or limestone-like sorbents. In the impregnated sorbents a reaction is to finish if the metal oxide layer were being entirely consumed by SO_2 without pore plugging. Practically this can not be complete, since the reaction proceeds only when the pore remains open and has any unreacted solid reactant. On the other hand in the limestone-like sorbent solid reactants are whole pellet itself. In the analysis of Dassori et al. [5] The effect of the averaged structural changes in the active solid (CuO) in the alumina matrix on the extent of reaction was included. They characterized the structural changes by three pa-

*To whom all correspondence should be addressed.

rameters: the ratio of the solid product ($CuSO_4$) molal volume to that of the solid reactant (CuO), the weight fraction of active solid, and the radial distribution of the active solid within the pellet. In general the evolution of pore or grain size distribution can not be represented by the simple averaged pore radius for such pores or grains.

The models that follow the evolution of a complete distribution of pore sizes with the extent of reaction when SO_2 reacts with the calcium oxide pellet have been presented by Christman and Edgar [6]. They did consider the effect of solid product buildup on the surface of pores. Performing a population balance over pore size distribution they generated a partial differential equation. They attained the numerical solution and compared the results with experimental data shown in the literature. In the study on the reaction of the impregnated adsorbents and the sulfur dioxide using distributed pore size model, Chung et al. [7] proved that the initial surface reaction rates varied with the impregnation concentration, but the activation energy was constant.

This work is concerned with extending the previous work of Chung et al. [3,7]. We, in extending the model, do not incorporate the averaged pore size in the reaction extent, nor stop calculation even when the pore plugging takes place. Furthermore, we suggest a partitioned pore structure model in which the optimum impregnation concentration could be estimated for the maximum utilization of cupric oxide impregnated in the alumina. Also we will present the transport mechanism which describes the sorption of SO_2 through porous alumina, the reduction in pore size, and the ultimate termination of the reaction due to the plugging of entire local pores by the product deposition.

FORMULATION OF PARTITIONED PORE STRUCTURE MODEL

1. Partitions of a single pore

The pore sizes of an alumina pellet can be partitioned into three regions: micro-, meso- and macropores. The pore size regimes of any partition may be chosen arbitrarily if it is reasonable for the pellet employed. We assume that the macro pores are mainly located on the outermost portion within the pellet, the meso on the next, and the micro on the innermost portion. After the process of impregnation has been completed, we assume that the number of pores per unit volume remains the same. The active solid is distributed along the radius of the pellet, and forms a reacting layer. A gaseous reactant diffuses into the pore and reacts with the active solid. As the reaction proceeds, the radius of pore changes. We assume the total pore volume of the pellet V comprises three portions: V_1 designating the micro pore volume, V_2 the meso, and V_3 the macro. The radial location in a single pellet between micro pores and meso pores will be [8]

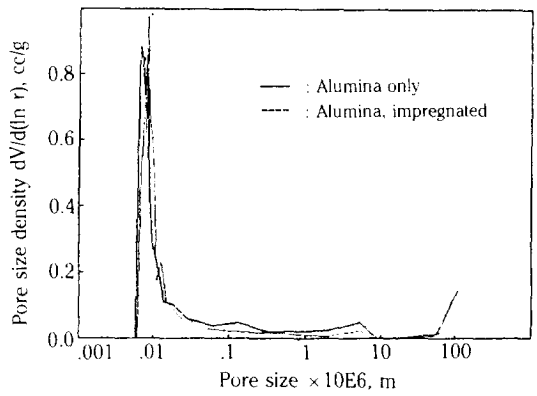

Fig. 1. Typical pore size density curves for the impregnated alumina prior to and after impregnation. The dotted line is that for the impregnated particle.

$$R_1 = \sqrt[3]{\frac{V_1}{V_1+V_2+V_3}}R_p. \tag{1}$$

Similarly the location at which the macro pore begins will be

$$R_2 = \sqrt[3]{\frac{V_1+V_2}{V_1+V_2+V_3}}R_p. \tag{2}$$

For equations (1) and (2), R_p denotes the pellet radius. Then the mean pore radius of a specific partition can be calculated from the pore size density curve as depicted in Figure 1. A geometric mean pore radius, $\bar{r}_j$ of the j-th partitioned group can be represented by

$$\bar{r}_j = \sqrt{\frac{V_j}{\Sigma(v_{i,j}/r^2_{i,j})}}, \quad \begin{matrix} i=1, 2, \cdots, n \\ j=1, 2, 3 \end{matrix} \tag{3}$$

where the subscript j denotes the partitioned group; 1 for the micro, 2 for the meso, and 3 for the macro, respectively. Also i designates individual pores, i.e., the i-th pore that has pore radius r_{ij} and pore volume, v_{ij} in the j-th partition. These forms can be conveniently extended when we enlarge the partitions. Let δ_{ij} be the thickness of impregnation of active reactant(CuO), covering the pores. The geometric mean thickness $\bar{\delta}_j$ of the j-th partition is related similarly to the mean pore radius by

$$\bar{\delta}_j = \bar{r}_j \left(\sqrt{V_j^o/V_j} - 1\right), \quad j = 1, 2, 3 \tag{4}$$

where V_j^o is the pore volume of the j-th partition prior to impregnation i.e., that of the pure alumina.

As the reaction proceeds the pore radius changes. A product layer will form on the walls of the cylindrical pore, creating new radii r_1 at the gas-solid interface and r_2 at the solid-solid interface between reactant and product. Here we assume that the product layer grows on both inner and outer sides in radial direction. The reaction will continue only if the pore has both gaseous reactant and active solid reactant. If the shrinking rate of r_1 at the pore entrance were extreme, the entrance is clogged by the solid product when the product molar volume is larger than the active solid.

Consider the chemical reaction is taking place in the embedded pore.

$$CuO + SO_2 + 1/2\, O_2 \rightarrow CuSO_4.$$

The reaction can be generalized if oxygen exists excessively.

$$\beta_1 A(s) + \beta_2 C(g) \rightarrow \beta_3 B(s) \tag{5}$$

According to Christman and Edgar[6] the inner radius r_1 of the product layer can be related to the outer radius r_2 and initial radius r_o by

$$r_1^2 = \alpha r_o^2 + (1-\alpha) r_2^2 \tag{6}$$

where

$$\alpha = \frac{\beta_3 V_B}{\beta_1 V_A} \tag{7}$$

α is the effective ratio of the molar volume of the solid product to that of reactant. They also developed the following differential equation in the cylindrical coordinates for the gaseous reactant with concentration $\hat{c}$ diffusing through the product layer in the radial direction [6].

$$\frac{\partial \hat{c}}{\partial t} = \frac{1}{r}\frac{\partial}{\partial r}\left(D_s r \frac{\partial \hat{c}}{\partial r}\right) \tag{8}$$

Applying the following boundary conditions to equation (8),

i) $\hat{c}|_{r=r_1} = c$

ii) $k_s \hat{c}|_{r=r_2} = -D_s \left.\dfrac{\partial \hat{c}}{\partial r}\right|_{r=r_2}$.

After having combined the pseudo steady state solution of equation (8) to the equation (6), they attained an expression for the rate of change of the outer radius r_2 which was r_o initially.

$$\left(\frac{\partial r_2}{\partial t}\right)_{r_o} = \frac{(\beta_1/\beta_2) V_A k_s c}{1 + r_2 (k_s/D_s) \ln (r_2/r_1)} \tag{9}$$

Initial conditions for equation (9) are $r_2 = r_1 = r_o$.
Also they expressed the rate of change of r_1 using equation (6) and (9).

$$\left(\frac{\partial r_1}{\partial t}\right)_{r_o} = \frac{(\beta_1/\beta_2) V_A k_s c}{1 + r_2 (k_s/D_s) \ln (r_2/r_1)} \left(\frac{1-\alpha}{r_2/r_1}\right). \tag{10}$$

We will use equations(9) and (10) for the evaluation of the changes of pore radii r_1 and r_2 with respect to time.

2. Material balance in a single pellet

In a specific pore, the composition of solute gas varies from point to point along the radial direction in spherical coordinates of a pellet. By referring to the elementary section dR of the single pore in the cylindrical coordinates, the accumulation rate of gas with concentration c in the differential section due to the difference between input and output by diffusion and the surface reaction taking place at the sharp interface can be represented by equation (11). For the systems involving diffusion and chemical reaction in a porous catalyst, it can be assumed that the diffusivity is not a function of pellet radius R. However, the diffusivity $D_{R,j}$ in the radial direction along a pore in a single pellet may vary significantly from the micro pore to the macro pore. In this region, the gas-solid reaction occurs so that the values should be discriminated for a specified j-th partition,

$$\frac{\partial c}{\partial t} = \frac{1}{R^2}\frac{\partial}{\partial R}\left(R^2 D_{R,j} \frac{\partial c}{\partial R}\right) - \frac{2}{r_2} f_s, \quad j = 1, 2, 3 \tag{11}$$

where f_s denotes the surface reaction rate per unit surface area of the sharp interface. Using the definition of the surface reaction rate, we can express f_s as

$$f_s = k_s \hat{c}|_{r=r_2}. \tag{12}$$

The continuity of concentration and flux at the boundaries where one partition contacts another must be satisfied by the following boundary conditions,

$$c|_{R_j -} = c|_{R_j +}, \qquad j = 1, 2 \quad \text{(11a,b)}$$

$$D_{R,j} \left.\frac{\partial c}{\partial R}\right|_{R=R_j -} = D_{R,j+1} \left.\frac{\partial c}{\partial R}\right|_{R_j +}, \quad j = 1, 2. \quad \text{(11c,d)}$$

The spherical symmetry for the concentration distribution and the continuity of flux at the outermost part of the sphere generate the following boundary conditions,

$$\frac{\partial c}{\partial R} = 0, \qquad R = 0 \quad \text{(11e)}$$

$$D_{R,3}\frac{\partial c}{\partial R}=k_g(c_b-c), \qquad R=R_p. \tag{11f}$$

Initial gas concentration, which is usually assumed to be zero, also gives the following condition,

$$c(t,R)=c_0(R), \quad t=0, \quad 0\le R\le R_p. \tag{11g}$$

The properties for c, r_1 and r_2 can be determined by a self consistent numerical method. The other macroscopic property of interest is the fractional conversion of reactant A to product B. The conversion can be expressed as a function of the resulting porosity as following;

$$x(R,t)=\frac{\varepsilon^o-\varepsilon(R,t)}{(1-\varepsilon^o)(\alpha-1)}. \tag{13}$$

3. Material balance in a fixed bed reactor

Consider a packed bed of pellets through which flue gases are passing and assume that the inlet concentration of the solute gas is so low that any reduction in its concentration causes a negligible change in the overall volume flow rate. Then the material balance of the gas with concentration c_b for the differential section dL of the reactor generates equation (14). In this equation, we assume that the rate of disappearence by adsorption onto pellets is equal to the rate of diffusion rate into the pellets.

$$\frac{\partial c_b}{\partial t}=D_L\frac{\partial^2 c_b}{\partial l^2}-U\frac{\partial c_b}{\partial l}-\frac{1-\varepsilon_b}{\varepsilon_b}\frac{3\varepsilon}{R_p}k_g(c_b-c|_{R_p}). \tag{14}$$

The diffusion rate to the inlet of the reactor can be equated with the mass transfer rate derived from the difference of concentrations as shown in equation (14a), while the concentration changes at the outlet are assumed to be negligible in equation (14b),

$$D_L\frac{\partial c_b}{\partial l}=k_g(c_b-c_o), \quad l=0 \tag{14a}$$

$$\frac{\partial c_b}{\partial l}=0, \qquad l=L. \tag{14b}$$

The concentration distribution at time zero can be expressed by

$$c_b(t,l)=c_{b0}(l), \quad t=0, \quad 0\le l\le L. \tag{14c}$$

4. Numerical solution

The solution of the model equations can be attained numerically. Park et al. [9] attempted to approximate the solution $r_2(t,r,l)$, and $c_b(t,r,l)$ and $c_b(t,l)$ by the collocation method employing the Hermite cubic basis function. They employed the variably located break points to increase the computing accuracy. Here is the brief description of the method, which requires the following basis steps.

1. Partitioning of the pore sizes in equation (3) according to the predetermined groups from pore density curves.
2. Solution of the evolution equation (9) to determine how the pore size distribution varies as a function of time.
3. Determination of the macroscopic properties (D, k, ε) as a function of time.
4. Solution of the mass balance, equation (11), to determine the radial concentration profile of the reacting gas in the pore.
5. Solution of the mass balance, equation (14), to determine the axial concentration profile of the reacting gas in the reactor.

Table 1. Physical and chemical properties of alumina obtained from Nishio Co., Japan

Pellet radius (m)	4.36×10^{-4}
Surface area (m^2/g)	2.26×10^2
Pore volume (cc/g)	0.3023
Packed density (g/cc)	0.86
Alumina	99.7%

EXPERIMENT

1. Preparation of solid adsorbent

Adsorbents were prepared by immersing alumina (Nishio KHO-9-20, Japan) in copper nitrate aqueous solution for 48 hours. The properties of the adsorbents are shown in Table 1.

The concentration of the impregnating solution, required to give the desired copper content, was calculated on the basis that all of the pores in the particles would be filled with the solution. The impregnated alumina was removed from the nitrate solution and quickly rinsed to remove any of the solution trapped between the particles. The particles were dried at 80°C for 48 hours and heated to 450°C in an air circulated muffle furnace to decompose the copper nitrate to the desired copper oxide. The copper content of the adsorbent was determined volumetrically by the potassium-iodine thiosulfate method. To assure the cupric oxide conversion X-ray diffractometer was used. The result of the X-ray analysis was so satisfactory that no trace of the cuprous oxide was found.

2. Packed bed reaction system

A simulated flue gas was supplied from the premixed pressurized gas cylinder. The SO_2 concentrations of the gas were fixed to 1000, 2000, and 3000 ppm with

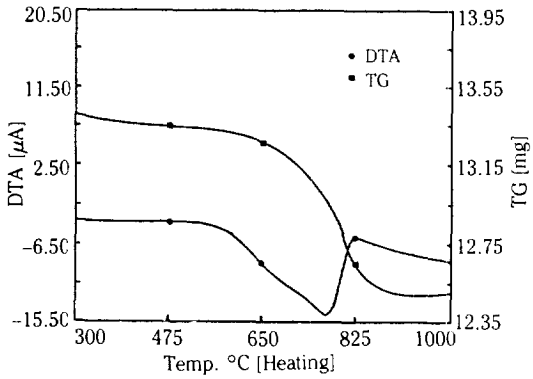

Fig. 2. Thermogram of reacted sorbent to determine the conversion.

air. The packed bed containing the adsorbents was placed in the gas chromatography oven (Shimadzu GC 3BT) that could control temperature from ambient to 450°C within 0.5°C precision. The inflowing stream gas was heated to the reactor temperature in a 50 cm long, 3 cm diameter coil of 4 m stainless steel tubing contained within the oven. Prior to sending the reacting gas, dried air was supplied into the reactor. After the temperature reached to the desired temperature the switching valve was opened manually to pass the reacting gas. At the same time the gas sampling valve at the outlet of the reactor operated to supply a vessel of 250 m*l* containing hydrogen peroxide solution. The solution in the vessel was sampled periodically. The SO_2 content of the solution was measured from the acidity of the solution. Meanwhile the gas was sampled into a syringe needle to analyse in the gas chromatography equipped with the thermal conductivity detector.

3. Pore structure measurement

A Micrometrics model 9300 mercury porosimeter was used to study the macro pore structure of the adsorbents in the pressure range of 1.5 to 30,000 psi. Pores of radii less than 17 Å were analysed by the adsorption technique using a Quantasorb System (Quantachrome Co.). Nitrogen adsorption at 77 K was measured, and isotherms were analysed by the BET equation. Figure 1 demonstrates the typical pore size density curve. In this figure, the solid curve corresponds to the density profile for the alumina prior to impregnation and the dotted curve for the impregnated one, respectively. Two curves are seen to be identical in the micro pore region, however, the humps shown in the macro and meso porous region are reduced and drifted to the micro porous region due to the layering effect by copper oxide.

4. Particle conversion measurement

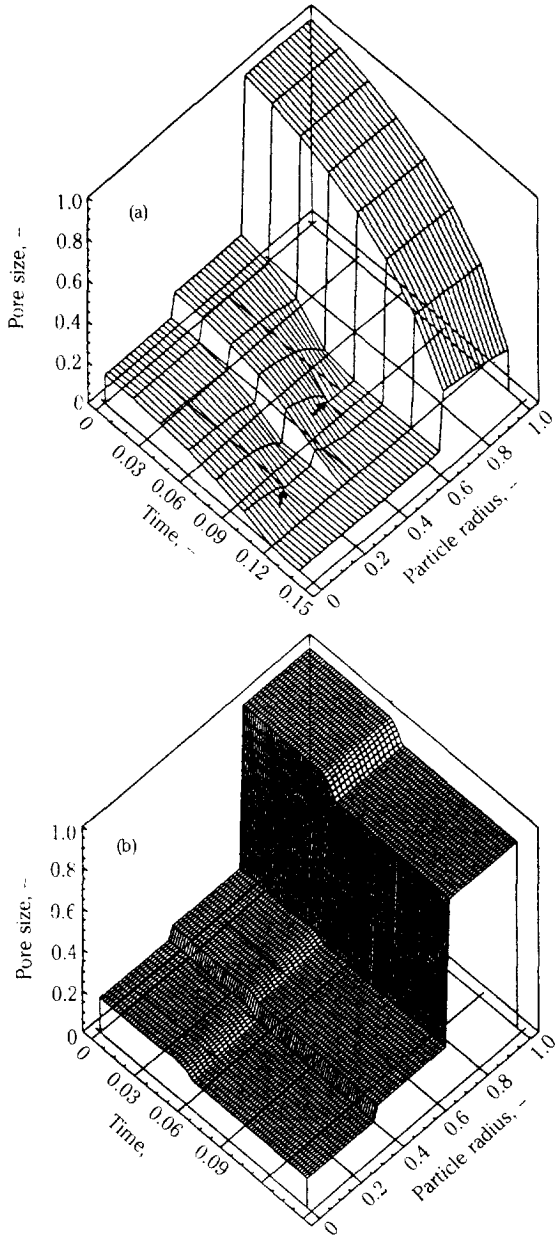

Fig. 3. Change of pore size of a pellet at the entrance of the reactor along with reaction time.

a: Showing micro and meso pores are clogging at arrow position.

b: Showing no clogging.

The conversion of particles in the reaction bed was measured by Seiko model SSC-5000 Thermo Analyzer (TG/DTA). To prepare partially reacted samples for the model identification, the reaction was terminated at

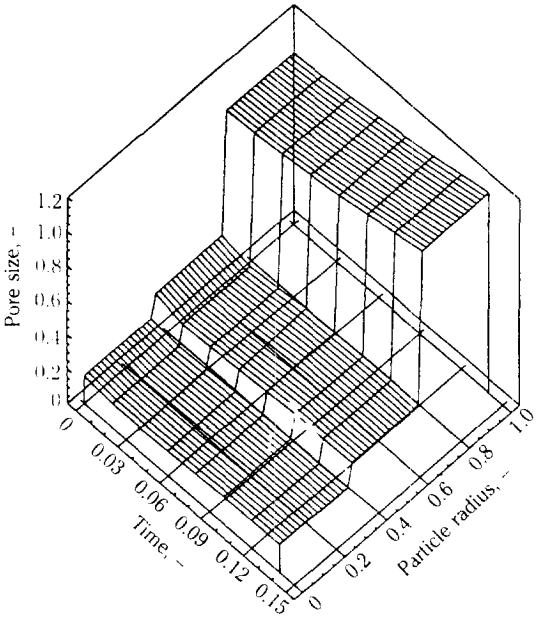

Fig. 4. Growth of product layer in pellet.

the desired conversion levels by purging dry air through the reaction chamber. Then the particle in the bed was sampled. Because of the difficulties in sampling from the proper bed height, the conversion measurement was limitted to the shallow bed height or to the top of the bed. Figure 2 shows the resulting thermogram. As this figure exhibits, it was difficult to assure the beginning temperature for the decomposition of the copper sulfate. It is necessary to confer the differential temperature curve.

RESULTS AND DISCUSSION

1. Pore size and concentration evolution in a pellet

The coefficients employed in this work are the surface reaction rate coefficients, the effective diffusion coefficients in bed and in pellet, the surface diffusion coefficients in product layer and the mass transfer coefficients as a function of temperature, flow rate and SO_2 concentration. The detailed definition for these parameters and the algorithm used here are listed elsewhere [7].

The change of poe size in a pellet at the entrance of the reactor along with the reaction time is depicted in Figure 3. In the high concentration of the impregnating solution, e.g., 8 mol// copper nitrate, the micro and the meso pores are clogging as shown in Figure 3a. In contrast to Figure 3a and 3b illustrates that the structural clogging was not detected even under the low concentration for the solution, e.g., 2 mol//. The

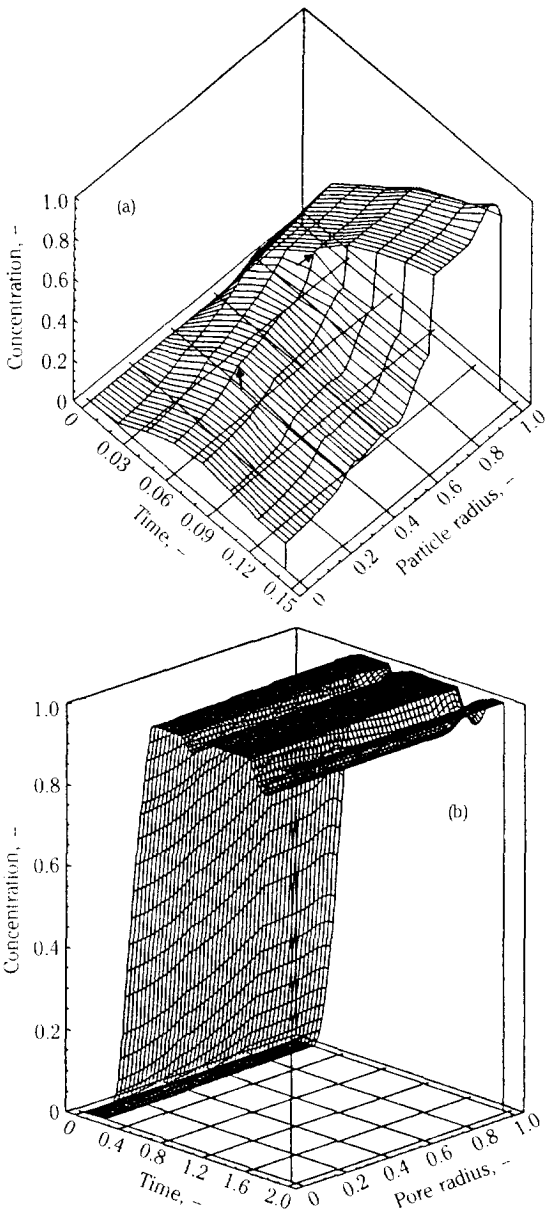

Fig. 5. Concentration changes in pellet.
a: Clogging case.
b: Unclogging case.

growth of product layer in the pellet pore is shown in Figure 4. Initially the outer most radius of the reacting surface was 1.0; it was enlarged to 1.2 at dimensionless time 0.12.

In Figure 5a and 5b, the concentration changes of SO_2 within the intraparticle pellet were plotted as a function of time and particle radius. These figures are closely related to the previous figures. Figure 5a for

the clogged case is corresponding to Figure 3a while Figure 5b for the unclogged case to Figure 3b, respectively. Initially the reacting gas diffuses thoroughly into the pore until being clogged.

This point is clearly illustrated in these figures. The concentration distribution of SO_2 for the clogged case (Figure 5a) is initially increased with the reaction time due to the free motion of gas molecule within the intrapellet. For the micro porous and the meso porous region, the transition time near the value 0.05 in dimensionless units indicates the structural change in the pores. After the transition time of pore clogging, the gradual decrease in the reaction rate is displayed in this figure. For the macro porous region, a similar characteristic behavior is observed until the transition time reaches. In this case of larger pores, SO_2 concentration is, however, increased after this time of pore closure. The concentration profile in the larger pores is more sensitive to the reaction time than that in the smaller pores. Also shown by arrows in this figure are the transition radius in dimensionless units of about 0.4 and 0.8. In the case of unclogging pores, this transitional behavior does not appear in the concentration profiles (Figure 5b). Under this condition, the reacting SO_2 from the bulk flow penetrates into the pore region, and consequently, these profiles do not exhibit any sudden cut-off of adsorption. Without the structural resistance in this case, the resulting SO_2 concentration increases continuously and approaches to the maximum saturation concentration.

SO_2 confined in the clogged pore reacts further until there is no more reactant left but it accumulates only on the outermost region. The solid reactant in the clogged pore ceases to react, with its conversion remaining at a low level. This was illustrated by a concentration gap in Figure 5a. Furthermore, it suggests the existence of an optimum impregnation concentration for maximizing the adsorption efficiency of the sorbent.

Two dimensional representation of pore size evolution and the concentration distribution are given in Figure 6a and 6b, respectively. Figure 6c shows both plots for comparison. The impregnated pore radii at the begining of adsorption are designated by arrows in Figure 6a. The product layer formed by the reaction shirinks the radius inside. The rate of shrink at the outer position is higher than that at the inner position since the incoming gas concentration is high. Therefore the shape of the shirinking pore changes gradually into an ellipsoid. The concentration distribution in a pore prior to, after, and at the instance of the meso pore clogging are marked by ▼, ▲, and ■, respectively.

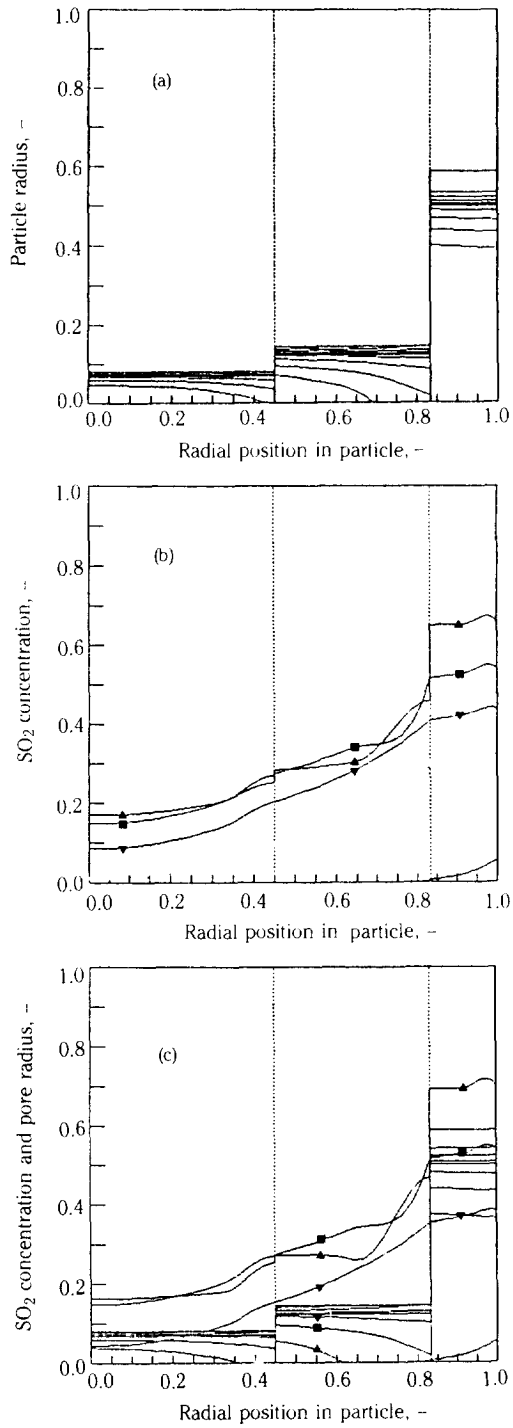

Fig. 6. Two dimensional representation of change in properties.

a: Pore size evolution.
b: Concentration change.
c: Both of pore size and concentration changes.

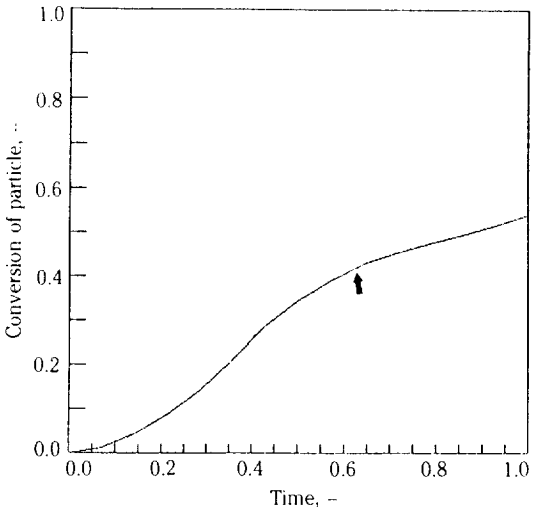

Fig. 7. Conversion of pellet at reactor entrance.

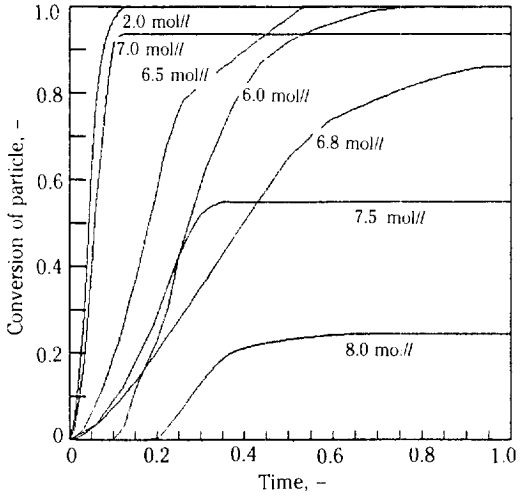

Fig. 8. Effects impregnation concentration on pellet conversion

The conversion of the particle at the reactor entrance can be seen from Figure 7. The rate of conversion decreases gradually from the time 0.6 at which the meso pore begins to clog as the arrow exhibits. The effect of the concentration of impregnation on the overall conversion of a single particle is illustrated in Figure 8. The thinly coated particle undergoes a complete conversion since the diffusion through the pore can reach the extreme end of the pore. As the concentration increases the conversion is incomplete due to the clogging effect. Concentration around 6.0 mol/l seems to be the optimum impregnation level if the SO_2 concentration is about 3000 ppm. For higher impregnation levels, the conversion rate drops down rapidly since most portions of the pore tend to be clogged. The conversion proceeds smoothly at the 6.0 mol/l, but at concentration as high as 6.5 mol/l the conversion rate changes as shown in Figure 8. The sudden slope change around time 0.2 in the 6.5 mol/l case is caused by the clogging at the interface between the macro and the meso pore. Even though the curve exhibits almost complete conversion, the slop change suggests that some cloggings are happening. Consequently it is concluded that the optimum impregnation concentration is 6.0 mol/l when the reacting SO_2 concentration is about 3000 ppm. If the SO_2 concentration were lower than 3000 ppm, the optimum concentration of the impregnation would become higher than 6.0 mol/l since the clogging would not occur on the concentration, and therefore the adsorbents with higher copper content can be used longer than the lower ones.

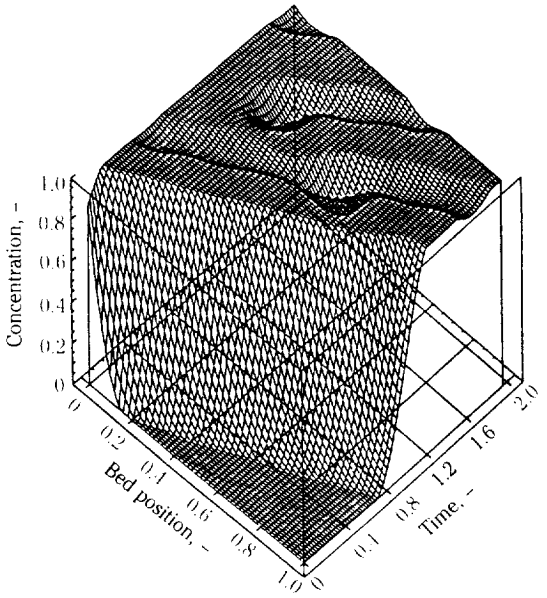

Fig. 9. Changes in concentration along with time in reactor bed.

2. Concentration change in bed and breakthrough curves

The change of concentration distribution along with time in the reactor bed is shown in Figure 9. The three dimensional drawing shows that the moving front of the distribution is shifting toward the exit of the reactor in the backward direction in the time axis of this figure. The fluctuation in the saturation region stems from the inability of spline functions to represent the abrupt change of concentrations since the larger mesh sizes were employed in the numerical

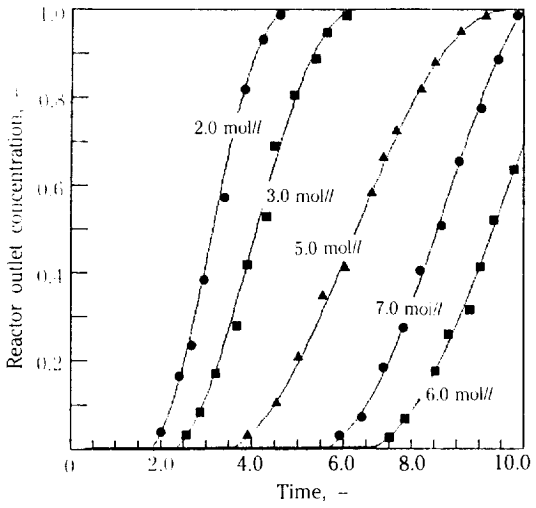

Fig. 10. Experimental and theoretical breakthrough curves.

solution. The breakthrough curve from the experiment and that from the solution are represented in Figure 10. Unit dimensionless time is equivalent to 15 minutes residence time in the reactor. As suggested in the previous discussions of the sorbent conversion, the breakthrough time defined as the time when the exit gas concentration reaches 5 percent of the inlet concentration prolonged to 6.8 dimensionless time at the 6.0 mol/l impregnation concentration. At concentrations higher than 6.0 mol/l the flow passes faster than the breakthrough time.

CONCLUSION

The partitioned pore structure model has been adapted to the sulfation of copper oxide impregnated in alumina, and the mechanism of SO_2 adsorption has been analysed theoretically and experimentally. In conclusion the impregnation concentration greatly affects the sorption capacity of the sorbent.

The optimum concentration of impregnation for the use of the alumina sorbent for the flue gas of around 3000 ppm has been proved to be about 6 mol/l copper nitrate aqueous solution.

ACKNOWLEDGEMENT

This work has been performed under the grant of Korea Research Foundation 1988, and the authors are grateful to the Foundation for the financial support.

NOMENCLATURE

c : bulk concentration in pellet pore
$\hat{c}$: concentration of gaseous reactant in solid product layer
c_0 : concentration of gas at the entrance of the reactor
c_b : concentration of gaseous reactant in reactor bed
D_L : dispersion coefficient of gaseous reactant in reactor bed
D_R : effective diffusion coefficient of gaseous reactant in pellet pore
$D_{R,j}$: effective diffusion coefficient in the j-th partitioned regime of pore
D_s : diffusion coefficient of gaseous reactant in product layer
f_s : surface reaction rate per unit surface of sharp interface
k_s : surface reaction rate constant
k_g : mass transfer coefficient at pellet surface
K_g : mass transfer coefficient at reactor inlet
l : axial position in reactor
$\bar{r}_j$: geometric mean pore radius of j-th partitioned group
$r_{i,j}$: individual radius of i-th pore in j-th partition
r_o : impregnated pore radius
r_1 : radius of pore during reaction
r_2 : radius of product layer
R : radial position of pellet
R_1 : radial location ending micro pore in pellet
R_2 : radial location ending meso pore in pellet
R_P : radius of pellet
$v_{i,j}$: individual volume of i-th pore in j-th partition
V_j^o : pore volume of j-th partition prior to impregnation
V_1, V_2, V_3: pore volume designating micro, meso and macro, respectively
V_A, V_B : molar volume of reactant A and product B, respectively
x : conversion of single pellet
α : molar volume ratio of solid product to solid reactant
$\beta_1, \beta_2, \beta_3$: stoichiometric coeffcient
$\delta_{i,j}$: thickness of impregnation of i-th pore in j-th partition
$\bar{\delta}_j$: geometric mean thickness of j-th partition
ε : porosity of pellet
ε^o : initial porosity of pellet
ε_b : bed porosity

REFERENCES

1. Dautzenberg, F.M., Naber, J.E. and van Ginneken, A.J.J.: *Chem. Eng. Prog.*, **67,** 86 (1971).

2. Yates, J.G. and Best, R.J.: *Ind. Eng. Chem., Process Des. Dev.*, **15,** 239 (1976).
3. Chung, S.H., Kim, D.C., Park, C.Y. and Cho, C.H.: *HWAHAK KONGHAK,* **27,** 767 (1989).
4. Simons, G.A. and Rawlins, W.T.: *Ind. Eng. Chem. Process Des. Dev.*, **19,** 565 (1980).
5. Dassori, C.G., Tierney, J.W. and Shah, Y.T.: *AIChE J.*, **34,** 1878 (1988).
6. Christman, P.G. and Edgar, T.F.: *AIChE J.*, **29,** 388 (1983).
7. Chung, S.H., Kim, D.C., Cho, C.H. and Park, C.Y.: *HWAHAK KONGHAK,* **28,** 184 (1990).
8. Chung, S.H.: Ph.D. Dissertation, Chonnam National Univ., Seoul, Korea (1990).
9. Park, C.Y., Lee, Y.C. and Chung, S.H.: *KJChE, submitted.*